IEEE Access
Multidisciplinary ⋮ Rapid Review ⋮ Open Access Journal

Received January 8, 2022, accepted January 19, 2022, date of publication January 26, 2022, date of current version February 8, 2022.

Digital Object Identifier 10.1109/ACCESS.2022.3146719

Non-Oscillatory Connectivity Approach for Classification of Autism Spectrum Disorder Subtypes Using Resting-State fMRI

ALISHBA SADIQ[1], MOHAMMED ISAM AL-HIYALI[1], NORASHIKIN YAHYA[1], TONG BOON TANG[1], (Senior Member, IEEE), AND DANISH M. KHAN[1,2], (Member, IEEE)

[1]Centre for Intelligent Signal & Imaging Research (CISIR), Electrical & Electronic Engineering Department, Universiti Teknologi PETRONAS, Bandar Seri Iskandar, Perak 32610, Malaysia
[2]Department of Telecommunications Engineering, NED University of Engineering and Technology, Karachi 75270, Pakistan

Corresponding author: Norashikin Yahya (norashikin_yahya@utp.edu.my)

This work was supported in part by the Ministry of Education Malaysia under Higher Institutional Centre of Excellence (HICoE) Grant awarded to the Centre for Intelligent Signal and Imaging Research (CISIR) and in part by Yayasan Universiti Teknologi PETRONAS under Grant YUTP-FRG 015LC0-292.

ABSTRACT Resting-state functional magnetic resonance imaging (rs-fMRI) is an efficient tool to measure brain connectivity and it can reveal patterns that distinguish autism spectrum disorder (ASD) from normal controls (NC). It is established that the fractal nature of neuroimaging signals will affect the estimation of brain's functional connectivity. Therefore, the ordinary correlation of rs-fMRI may not provide the original neuronal activity of the brain. In this work, the non-oscillatory brain connectivity method is proposed to distinguish subtypes of ASD from NC. The three subtypes of ASD namely autistic disorder (ATD), Asperger's disorder (APD), and Pervasive developmental disorder-not other specified (PDD) are classified from NC by extracting the non-oscillatory connectivity from the BOLD rs-fMRI signal. A number of significant connections are extracted by utilizing the *p*-value analysis and these significant connections are fed to machine learning (ML) classifiers for classification of ASD subtypes against normal control. The performance for binary classification is recorded at accuracy of 98.6%, 97.2%, 97.2%, respectively, for ATD vs. NC, APD vs. NC and PDD vs. NC. Whereas, for multiclass (ATD, APD, PDD and NC), the best accuracy is 88.9%. Both binary and multiclass classification outperformed the conventional Pearson correlation-based connectivity and benchmark approaches in terms of accuracy, sensitivity, specificity. This work demonstrates the great potential of non-oscillatory connectivity approaches, not only for autism diagnosis but also for other neurological disorders.

INDEX TERMS Asperger's disorder, pervasive developmental disorder, fractal free, neurodevelopmental, Pearson correlation, machine learning.

I. INTRODUCTION

Autism spectrum disorder (ASD) is a complex neurodevelopmental disorder that disturbs various abilities of a person which includes social and communication challenges, repetitive behaviour, speech delay, etc. Because the abnormality usually appears before a kid reaches the age of three, it might be difficult to notice and it can last throughout a person's life. Therefore, early ASD identification can help to address the above-mentioned difficulties and enhance the quality of life for people with ASD and their families. The Centre for Disease Control and Prevention (CDC) estimates that one out of every 54 children in the United States has autism [1]. According to World Health Organization (WHO) data, one out of every 160 children in the world has ASD [2]. With increasing prevalence of ASD, it is important to diagnose ASD in the early stages to mitigate the consequences in the later stages.

ASD is now an umbrella term according to American Psychiatric Association (APA) after 2013 according to the diagnostic and statistical manual of mental disorders (DSM-5) [3], ASD covers the following conditions: 1) Autistic disorder (ATD), 2) Asperger's disorder (APD) and 3) Pervasive developmental disorder-not otherwise specified

The associate editor coordinating the review of this manuscript and approving it for publication was Yiqi Liu.

(PDD). Autistic children exhibit a variety of characteristics, including resistance to change, aggression, and self-injurious behaviour [4]. APD, which is one of the wider categories of ASD modestly affects children, and they have normal cognitive and verbal abilities. They do, however, have more difficulty with social skills than other types of ASD, and they repeat the same activities and actions that they enjoy. Children with APD may experience fewer emotions and express themselves less. However, PDD is a collection of disorders marked by difficulties with social interaction, verbal and nonverbal communication, imaginative activity, and a small number of repeated interests and activities.

Early diagnosis of ASD can be helpful for children and their families and it can mitigate the symptoms associated with the disorder. Although it is a challenging task, the earlier it is diagnosed, the better it is for the individual. Research suggests that early autism diagnosis and intervention methods are likely to have significant long-term favourable impacts on symptoms and subsequent skills [5]–[7].

Diagnosis of Autism is a challenging task as there is no standard test or tool available for the correct diagnosis of the disorder [8]. Doctors observe the children's behaviour or take the history of the child from parents' interviews. There are two diagnostic tools available for autism diagnosis, it includes Autism Diagnostic Observation Schedule (ADOS) which is based on tasks that involve social interaction. The examiner observes the person under assessment and gives scores based on observation. An associated measure, the Autism Diagnostic Interview-Revised (ADI-R), is a structured interview with the subject's parents that covers the subject's entire developmental history [9]. As these assessment tools are based on observation, there is a high risk of false positives in individuals with other psychological disorders. In particular, adults with psychosis have a higher rate of false positives [10]. Similar false diagnosis can be seen in case of childhood-onset schizophrenia [11], attention/deficit hyperactivity disorder (ADHD) [12] etc. Clinical assessments and behavioural observations are used to diagnose ASD. However, since clinical scores are vague, it is necessary to uncover accurate brain biomarkers and automate the ASD diagnosis procedure [13].

A. RELATED WORK

Several studies have revealed that brain connectivity can be a substantial biomarker for ASD classification. It can reveal patterns that distinguish ASD from healthy controls [14]–[16]. Resting-state functional Magnetic Resonance Imaging (rs-fMRI) is a powerful method to examine brain connectivity patterns. Classification studies using rs-fMRI showed connectivity differences between ASD and controls [17]–[19]. In [17], Antonis *et al.* used rs-fMRI to classify ASD. Functional connectivity was used as a feature vector to be fed to the machine learning (ML) classifier, utilizing the RBF kernel and yielded the highest accuracy of 69.77%. Rajat Mani *et al.* in [18], used the temporal statistics of rs-fMRI data for the classification of ASD achieving the highest accuracy of not more than 66%. Adora *et al.* in [19], used rs-fMRI with mutual connectivity analysis to find the differences among various brain regions related to ASD and controls. They achieved the mean accuracy between 70%-81%

In development of automatic diagnosis of ASD using BOLD fMRI signals, two main type of extracted feature are considered, either dynamic [20]–[22] or static functional connectivity (FC) [23]–[29]. However, for dynamic FC [20]–[22], the methods were tested on a relatively small sample size of less than 100. Several combinations of static FC fMRI feature and classifier have been applied in the literature to determine the functional connectivity among brain nodes from rs-fMRI data then applied as input to machine learning models. Pearson correlation method is widely employed to estimate the temporal dependency coefficients between the brain nodes which are reflected in the association and direction connectivity between brain nodes. Chen *et al.* [23] used Pearson correlation coefficients as input to Support Vector Machine (SVM), achieving 79% accuracy for ASD classification. Recently, Chaitra *et al.* [30] attempted to develop the ASD classification performance by applying Pearson correlation coefficients with other complex brain networks matrices as input to Recursive-Cluster-Elimination-SVM (RCE-SVM). However, their method achieved 70.1% accuracy for ASD diagnosis which is lower than the previous study [23]. In another work by Abraham *et al.* [24], covariance matrices are used to estimate the FC between brain nodes and become the input features to an SVM classifier giving 67% accuracy.

Known for its excellent result in various automated classification [31], [32], deep learning approaches are also employed to improve the ASD classification based on FC patterns. Heinsfeld, *et al.* [25], extracted the FC based on the Pearson correlation between voxels time series and feeds to deep neural networks (DNN), giving 70% classification accuracy. above-cited studies applied the Pearson correlation coefficients as input vectors to the model, while Sherkatghanad, *et al.* [28], converted the Pearson correlation coefficients as 2D-matrix and used them as input to the Convolutional Neural Network (CNN) given 70.2% ASD vs. NC classification accuracy. In [26], Eslami, *et al.* utilized anti-correlated and highly correlated functional connections as the feature vector and trained on a joint learning architecture using an autoencoder and a single layer perceptron (SLP) which results in 70% accuracy in classification of ASD vs. NC. However, the findings of the above-cited studies have reported ASD diagnostic with the best accuracy of 79% which means that more research in this area is required in improving the ASD classification.

The use of neuroimaging techniques, such as fMRI [26], [33], electroencephalography [34] and magnetoencephalography [35], [36], allows indirect assessments of brain neuronal activity. However, it is not straightforward to extract the pure neuronal signal as neuroimaging signals are affected by physiological influences and it is essential to

consider this phenomenon when developing a classification algorithm. It is established in [37]–[42] that neuroimaging signals exhibit fractal behaviour i.e., having self-similarity and power-scaling properties. The fractal nature may originate from the cardiac oscillations [43], respiration [44], system noise and many more. This nature has an impact on brain connectivity patterns, leading us to look for a fractal-free brain signal to recover the pure neuronal activity. In this research, we extend the idea proposed by Wonsang *et al.* [37] in 2012 to the classification of ASD subtypes vs. controls based on fractal free signals i.e., non-fractal connectivity. To this date, the non-fractal, here termed as non-oscillatory connectivity has not been applied for classification of autism subtypes from normal controls.

The main contributions of the proposed research are as follows. In this work, the BOLD time series extracted from the rs-fMRI signal is used to find the non-oscillatory connectivity for the classification of autism subtypes from healthy controls. The proposed approach is expected to provide excellent results as the non-oscillatory signals provide a cleaned neuronal signal of the brain giving more accurate brain connectivity patterns. The method utilized BOLD time series signals extracted from 116 regions based on AAL atlas, thus giving a 116×116 symmetric connectivity matrix with zero diagonal values. The p-values analysis is used to find the most significant connections giving insights on how informative the connectivity patterns in discriminating between autism subtypes and normal controls. Several ML classifiers are tested to evaluate the performance of the proposed method and compared with Pearson correlation connectivity to demonstrate the excellent performance of the proposed method.

The remainder of the paper is organized as follows. Section II represents the modelling of the long memory process of rs-fMRI signal. In section III, methodology for development of the classification algorithm is shown including details of the dataset and derivation of the non-oscillatory connectivity. In section IV, results on the investigations of the proposed approach for the classification of autism subtypes and normal controls are presented together with the statistical analysis and discussion on the classification performance using the best ML classifier. In particular, our investigation is divided into two parts; 1) multiclass classification of ASD subtypes using 36-subject perclass and 2) binary classification using 505-ASD vs 530-NC subjects.

II. LONG MEMORY MODEL OF MULTIVARIATE rs-fMRI SIGNALS

We begin the modelling of rs-fMRI signals using a univariate approach prior to extension to the multivariate scenario. Here, the definition of long memory process is based on the general formalism established in [45], [46]. Let $c(t)$ be a real valued discrete process of length L with $s(t)$, a process called short memory having the spectral density $S_s(t)$ is given as:

$$s(t) = (1 - Q)^m c(t) \tag{1}$$

where $0 < m < 1/2$ and Q is defined as the back shift operator. The fractal behaviour is controlled by the 'm' parameter such that if $0 < m < 1/2$ the process $s(t)$ is said to be a stationary long memory process, while $m > 1/2$ is for a nonstationary process. Also, if $m = 0$ the process turns into a white noise. $c(t)$, which is the convolution of $s(t)$ and the long memory filter, $k(t)$ given as follows:

$$c(t) = \sum_{\tau=0}^{\infty} k(\tau) s(t - \tau) \tag{2}$$

where

$$k(t) := \frac{m\Gamma(m + t)}{\Gamma(m + 1)\Gamma(t + 1)}, \tag{3}$$

if $-\frac{1}{2} < m < \frac{1}{2}$, the spectral density of $c(t)$ can be written as

$$S_c(f) = |1 - e^{-jf}|^{-2m} S_s(f). \tag{4}$$

For the multivariate case of long memory model, the univariate case can be expanded. A w-vector real valued process $\boldsymbol{C}(t)$ given by:

$$\begin{pmatrix} (1 - Q)^{m_1} & & 0 \\ & \ddots & \\ 0 & & (1 - Q)^{m_w} \end{pmatrix} \begin{pmatrix} c_1(t) \\ \vdots \\ c_w(t) \end{pmatrix} = \begin{pmatrix} s_1(t) \\ \vdots \\ s_w(t) \end{pmatrix}, \tag{5}$$

where $\mathbf{S}(t) = (s_1(t), \ldots, s_w(t))$ shows a multivariate stationary process and the spectral density of $\boldsymbol{C}(t)$ is $\boldsymbol{S}(f) = [S_{p,q}(f)]$ is limited to $(-\pi, \pi)$. For $-\frac{1}{2} < m_d < \frac{1}{2}$, the spectral density of $\boldsymbol{S}$ is given as

$$\boldsymbol{S}(f) = \boldsymbol{\Theta}(f)\boldsymbol{S_s}(f)\boldsymbol{\Theta}^*(f), \tag{6}$$

where

$$\boldsymbol{\Theta}(f) = \begin{pmatrix} (1 - e^{jf})^{-m_1} & & 0 \\ & \ddots & \\ 0 & & (1 - e^{jf})^{-m_w} \end{pmatrix}. \tag{7}$$

Given that, $0 < m_d < \frac{1}{2}$ for $d = 1, 2, \ldots w$, $\mathbf{C}(t)$ is considered to be a stationary long-memory process having memory parameter $\boldsymbol{m} = (m_1, \ldots, m_w)$. Assuming $\mathbf{S}(t)$ to be a vector auto-regressive moving average (ARMA) process, $\mathbf{C}(t)$ eventually becomes a multivariate ARFIMA process. However, on the other hand, if $\mathbf{S}(t)$ is a vector of $i.i.d$ random variable, i.e.

$$S(t) \overset{i.i.d.}{\sim} L\left(0, \sum\nolimits_s\right). \tag{8}$$

$\mathbf{C}(t)$, becomes a multivariate fractionally integrated noise (mFIN). Now, the cross-spectral density of $c_p(t)$ and $c_q(t)$ is given as

$$S_{p,q}(f) = \psi_{p,q}(1 - e^{jf})^{-m_p}(1 - e^{-jf})^{-m_q}, \tag{9}$$

where $\psi_{p,q}$ is the (p, q)-th element of $\sum_s$.

TABLE 1. Demographic information of autism subtypes and normal control subjects according to gender and age.

Class	Gender (M/F)	Age (year)
ATD	29/7	12.02 ± 2.44
APD	31/5	17.51 ± 9.56
PDD	31/5	18.11 ± 11.54
NC	10/26	15.05 ± 6.73

III. METHODOLOGY

The schematic diagram of the proposed approach for the classification of subtypes of ASD against NC using neuroimaging data is shown in Figure 1 and presented in detail in this section. First, the rs-fMRI data is pre-processed following the standard procedure as it is the necessary step for further procedure. Then, defining the region of interest (ROI) and time-series extraction from 116 regions based on AAL atlas, followed by connectivity matrix extraction. Two types of connectivities are extracted namely, non-oscillatory and Pearson correlation. Pearson correlation-based connectivity is used for comparison and to show the efficacy of the proposed method. The machine learning classifiers are trained, and the parameters are optimized using a cross-validation (CV) framework.

A. RESTING-STATE fMRI DATASET

This work is carried out on resting-state fMRI data of equal size comprising 3 autism subtypes, ATD, APD, PDD as well as the normal controls. Each class has 36 subjects and the demographic detail of the subjects is shown in Table 1. The dataset is downloaded from the publicly available dataset of Autism Brain Image Data Exchange (ABIDE) [47]. As given in Table 1, there are more male subjects for the autism subtypes, with the ratio of male-to-female equal to 0.75:0.25. In contrast, the normal controls have more female subjects which is at 72.22% compared to 27.77% of male subjects. The age range of the subject is between 12 to 15 years old. The MRI scanning protocol and the location of data collection are provided in Table 2.

B. DATA PRE-PROCESSING AND EXTRACTION OF BOLD TIME-SERIES SIGNALS

Data pre-processing is an essential step prior to further investigation and statistical analysis of fMRI data as it removes the undesired artefacts and translates the data into a standard format. Connectivity toolbox (CONN) [48] is used to pre-process the data by performing realignment, slice-time correction, co-registration, normalization and smoothing. The subsequent processing is using the Data Processing & Analysis for (Resting-State) Brain Imaging (DPABI) toolbox [49] for extracting the BOLD time series from 116 nodes as defined by the AAL brain atlas.

The ABIDE dataset is a collection of rs-fMRI from multiple sites, using different type of scanners and protocol as listed in Table 2. Therefore, the signals vary in terms of the number of time-points. Selected brain regions comprising 116 nodes for extraction of BOLD time-series are based on AAL atlas [50]. With signals from 116 nodes, each subject will generate a connectivity matrix having a size of 116×116.

C. CONNECTIVITY MATRICES

1) PEARSON CORRELATION BASED CONNECTIVITY

Pearson Correlation Coefficient (PCC) of neuroimaging signals is a standard way to measure the functional connectivity between different regions, providing useful information on brain's activity [51]. The PCC between two time series can be calculated by finding the covariance between two time series and dividing it by the product of its standard deviation. If $c_p(t)$ and $c_q(t)$ denote the BOLD signal from region x and y, respectively, then the PCC of the two regions is

$$\beta_{c_p,c_q} = \frac{cov(c_p, c_q)}{\sigma_{c_p}\sigma_{c_q}}, \tag{10}$$

where cov denotes the covariance. The standard deviation is given by the symbol σ_p and σ_q for $c_p(t)$ and $c_q(t)$, respectively. The covariance can be calculated by subtracting the mean from time series and taking is expectation

$$cov(c_p, c_q) = E[(c_p - \mu_p)(c_q - \mu_q)], \tag{11}$$

where $E[.]$ is the expectation operator and μ_p and μ_q are the mean of $c_p(t)$ and $c_q(t)$, respectively.

2) NON-OSCILLATORY CONNECTIVITY (NOC)

The multivariate long memory model explained in Section II provides the concept of non-oscillatory connectivity, defined as the covariance of short memory signals. Consider $\mathbf{C}(t)$ to be an mFIN process having the memory parameter m, and $\mathbf{S}(t)$ is a short memory function of $\mathbf{C}(t)$ given in (5). The non-oscillatory connectivity of $c_p(t)$ and $c_q(t)$ is described as

$$A_{p,q} = \frac{\psi_{p,q}}{\sqrt{\psi_{p,p}\psi_{q,q}}}, \tag{12}$$

where $\psi_{p,q}$ represents the covariance of $s_p(t)$, and $s_q(t)$; that is, $\psi_{p,q} := E[c_p(1)c_q(1)]$.

Particularly, the NOC matrix requires the estimation of short memory covariance as shown in (12) and memory parameters m_p and m_q. The likelihood function for the estimation of the memory parameter was proposed by Yu *et al.* in [37]. For memory parameter m_p, the maximum likelihood function is given by

$$B\left(\hat{m}_p, \hat{\psi}_p | c_p(t)\right) := \frac{1}{(2\pi)^{L/2}|\Sigma_p|^{1/2}} e^{-c^T \Sigma_p^{-1} c/2}, \tag{13}$$

where, the matrix Σ_p denotes the covariance matrix of $c_p(t)$.

The estimation of short-memory covariance for NOC matrix is obtained by using the linearity of wavelet covariance over scales given as

$$\hat{\psi}_{p,q} = \frac{2^{\hat{b}_{p,q}-1}}{D_{p,q}\cos\left(\frac{\pi}{2}(c_p - c_q)\right)}(2\pi)^{c_p+c_q}, \tag{14}$$

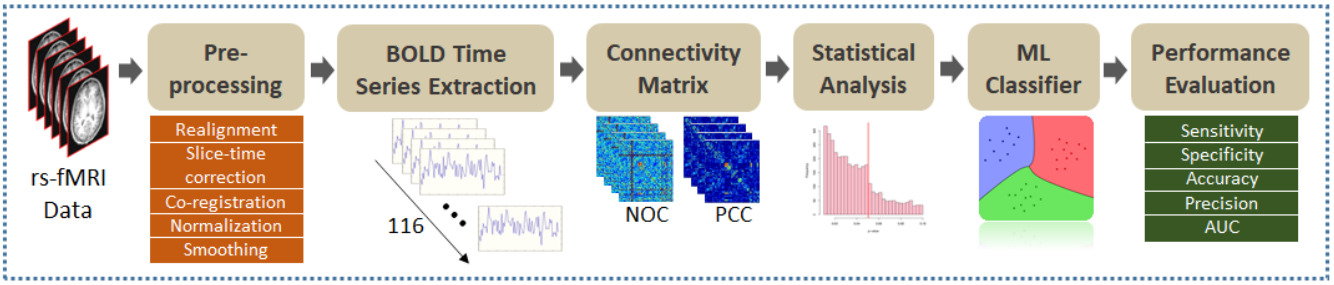

FIGURE 1. Methodology for classification of autism subtypes using non-oscillatory connectivity (NOC) of rs-fMRI signals.

TABLE 2. Data acquisition protocol details for autism subtypes and NC dataset from ABIDE database, acquired using 3T-MRI scanner.

Site	Country	Vendor	Voxel size	Flip angle (mm)	TR (sec)	Time-points (sec)	Subjects				Total Per Site
							ATD	APD	PDD	NC	
NYU	USA	Siemens	1.3	7	2	175	9	8	5	9	31
SBL	Netherlands	Philips	1	8	2.2	195	9	5	6	9	29
SDSU	USA	GE	1	4.5	2	175	9	6	2	9	26
Trinity	Ireland	Philips	1	8	2	145	-	4	7	-	11
Yale	USA	Siemens	1	9	2	195	9	5	14	9	37
USM	USA	Siemens	1	9	2	235	-	-	1	-	1
KKI	USA	Philips	1	9	2.5	151	-	8	-	-	8
UM	USA	GE	1.2	15	2	295	-	-	1	-	1
						Total	**36**	**36**	**36**	**36**	**144**

Legend: NYU: New York University, SBL: Social Brain lab, SDSU: San Diego State University, Trinity: Trinity College Institute of Neuroscience, Yale: Yale School of Medicine, USM: University of Utah School of Medicine, KKI: Kennedy Krieger Institute, UM: University of Michigan, TR:Repetition Time.

TABLE 3. Data acquisition protocol details of autism subtypes and NC dataset from ABIDE database, acquired using 3T-MRI scanner.

Site	Country	Vendor	Time-points	ASD	NC	Total Per Site
SDSU	USA	GE	175	14	22	36
STANFORD	USA	GE	235	19	20	39
UM	USA	GE	295	66	74	140
KKI	USA	Philips	151	20	28	48
LEUVEN	Belgium	Philips	245	29	34	63
SBL	Netherlands	Philips	195	15	15	30
TRINITY	Ireland	Philips	145	22	25	47
CALTECH	USA	Siemens	145	19	18	37
CMU	USA	Siemens	315	14	13	27
MAX	Germany	Siemens	115	24	28	52
NYU	USA	Siemens	175	75	100	175
OHSU	USA	Siemens	77	12	14	26
OLIN	USA	Siemens	215	19	15	34
PITT	USA	Siemens	195	29	27	56
UCLA	USA	Siemens	115	54	44	98
USM	USA	Siemens	235	46	25	71
YALE	USA	Siemens	195	28	28	56
Overall	-	-		505	530	1035

Legend: NYU: New York University, SBL: Social Brain lab, SDSU: San Diego State University, Trinity: Trinity College Institute of Neuroscience, Yale: Yale School of Medicine, USM: University of Utah School of Medicine, KKI: Kennedy Krieger Institute, UM: University of Michigan, CMU: Carnegie Mellon University, MAX: Ludwig Maximilian University of Munich, OLIN: Olin Center, Institute of Living at Hartford Hospital, OHSU: Oregon Health and Science University, StANFORD: Stanford University, UCLA: University of California,Los Angeles, LEUVEN: University of Leuven, PITI: University of Pittsburgh School of Medicine

where

$$\hat{b}_{p,q} = \frac{1}{R}\sum_{r=1}^{R}[\log_2 \hat{\upsilon}_{p,q}(f) - (c_p + c_q)f], \tag{15}$$

$$D_{p,q} := \frac{1 - 2^{c_p + c_q - 1}}{1 - c_p - c_q}. \tag{16}$$

Given the estimated short-memory covariance in (14), the non-oscillatory connectivity of $c_p(t)$ and $c_q(t)$, $\hat{A}_{p,q}$ of can be estimated as follows

$$\hat{A}_{p,q} = \frac{\hat{\psi}_{p,q}}{\sqrt{\hat{\psi}_{p,p}\hat{\psi}_{q,q}}}. \tag{17}$$

For visual representation, a sample of ATD, APD and PDD and NC connectivity matrices for NOC and PCC are shown in Figure 2.

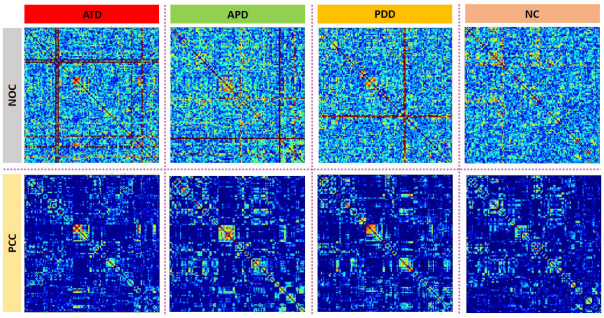

FIGURE 2. Sample of 116 × 116 non-oscillatory connectivity (NOC) and Pearson correlation connectivity (PCC) matrices for autism subtypes and normal control.

Algorithm 1 Method of Finding the Top-Ranked Features in Discriminating ASD Subtypes and NC Using p-Value Analysis

1) Let $FC \in \mathbb{R}^{1\times 6670}$ be the connectivity feature vector of the 160-timepoint × 116-region BOLD time series of one subject and τ_p is the selected p-value.
2) Arrangement of the feature vector for ASD and NC classes at 36 subjects per class producing 6670×36-feature vector
3) Find p-value of each connection
   if p-value $\leq \tau_p$
      save connection at S
   else $S =$ empty
4) Now, use S top-ranked features for classification

D. SELECTION OF HIGHLY DISTINCTIVE FUNCTIONAL CONNECTIVITY

From 116 brain regions, the size of the connectivity matrix is 116 × 116 which makes the number of total connections equals $116^2 = 13456$. However, since the matrix is symmetric with respect to the diagonal elements, where the connection from node A/B to node B/A are the same, the connectivity values to be considered are either the elements of upper or lower diagonal, excluding the diagonal elements. Hence, the length of the connectivity feature vector is $(116^2 - 116)/2 = 6670$.

For the 36 subjects per class, using a full-length feature vector of 6670-length may result in poor classification accuracy since this will result in a curse of dimensionality. Besides, not all connectivity carries discriminative information in differentiating the ASD subtypes and NC, hence, to reduce this large number of connections, p-value analysis is used. With a reduced feature vector, this will help to eliminate the least significant features from the data and thereby reduce the computational cost. Method to determine the p values is given in Algorithm 1.

E. CLASSIFICATION

Several ML classifiers have been utilized to evaluate the performance of the NOC-based ASD classification method. This includes SVM linear discriminant, naive Bayes, fine and cosine KNN and ensemble subspace discriminant. Selection of optimal machine learning hyperparameters for SVM, KNN and subspace discriminant ensemble is achieved by using Bayesian optimization that minimizes the CV loss as the objective function.

From the Bayesian optimization, the best performance of SVM is achieved using the cubic kernel function. The KNN classifier is run using 11-neighbour and cosine distance metric. Lastly, the subspace discriminant ensemble is used with a linear discriminant learner type of 30 learners and 410 subspace dimension. Decision of the output is based on majority voting rule.

F. PERFORMANCE MEASURES

The confusion matrix is used to calculate the following performance measures as listed below.

$$\text{Sensitivity (Sen)} = \frac{TP}{TP + FN} \tag{18}$$

$$\text{Specificity (Spe)} = \frac{TN}{TN + FP} \tag{19}$$

$$\text{Accuracy (Acc)} = \frac{TP + TN}{TP + TN + FP + FN} \tag{20}$$

$$\text{Precision (Pre)} = \frac{TP}{TP + FP} \tag{21}$$

where, TP is true positive, TN is true negative, FP is false positive, and FN is false negative.

However, for multiclass classification, the accuracy measure in equation (20) is calculated independently as macro accuracy which is defined as an accuracy computed for each class separately [52] The TP, TN, FP, and FN for each class can be calculated by using a confusion matrix. A Similar approach is used for calculation of macro sensitivity, specificity, and precision.

IV. RESULT AND DISCUSSION

In this section, the performance of the proposed method is evaluated for the classification of autism subtypes i.e., ATD, APD, PDD, and NC, respectively. The comparisons are made with the baseline approach i.e., Pearson-based connectivity. The algorithm is tested for 10-fold CV. Data from 144 subjects are used for the classification task using connectivity matrices based on non-oscillatory connectivity (NOC) and Pearson correlation connectivity (PCC). The evaluation of the ASD ML algorithms begin with multiclass ASD classification then followed by 2-class classification

The pre-processing of fMRI signals is by using the connectivity toolbox (CONN) [48] and statistical parametric mapping (SPM12) [53] implemented on the Matlab platform. For the extraction of BOLD time-series, Data Processing & Analysis for (Resting-State) Brain Imaging (DPABI) toolbox [49] is used. The training and testing of the ML algorithm is performed on a Windows 10–based computer powered by an octa-core processor (Intel Core i7-9700 CPU) and installed with 32 GB RAM with activated parallel computing (Matlab function).

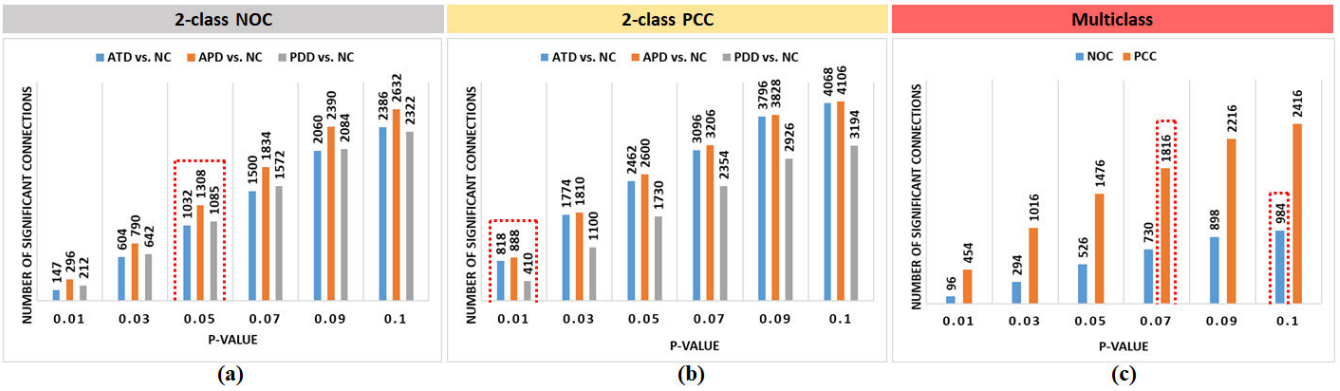

FIGURE 3. Significant connections of 2-class (a) NOC, (b) PCC and (c) multiclass, extracted at different p values. The significant connections that result in the best performance for NOC and PCC as determined from Table 4 and 5 are highlighted in a red dashed-box.

A. SELECTION OF TOP-RANKED FEATURES USING p-VALUE ANALYSIS

The connectivity from 116 regions generates a 6670-dimension feature vector which is a relatively large dimension compared to the number of subjects per class. This high dimensional feature vector will increase the complexity for the ML classifier to perform the classification task correctly. To remove the less informative connections and utilize the most significant connections, the p-value analysis is used to observe the importance of each connection for NOC and PCC.

In this section, the number of significant connections, S for binary and multiclass classification are determined for both NOC and PCC using p-value analysis as described in Section III-D. Figure 3, shows the number of S, as the p values is increased from 0.01 to 0.1 for binary and multiclass classification. In general, for each ASD subtype vs. NC as well as multiclass classification, the number of S for NOC is always lower compared to PCC. This may be attributed to the better representation of the brain's neural activities by the NOC since the signals used for generating NOC are free from oscillatory components generated by other physiological systems such as cardiac oscillations and also from system noise. The better representation of the brain's neural activities by the NOC will be useful in discriminating the ASD subtypes and NC and can be confirmed in the classification tasks, covered in the next 3 sections.

For better assessment on the 2-class and multiclass classification at different p-value, the classification performance using NOC and PCC trained on cubic SVM using S at increasing p values are evaluated. The classification accuracy values obtained using 10-fold CV are listed in Table 4 and Table 5, for 2-class and multiclass, respectively.

From Table 4, it can be seen that for NOC, the highest accuracy is achieved when $p \leq 0.05$ which is 98.6% for ATD vs. NC and 97.2% for the other two ASD subtypes versus NC. However, for PCC, the accuracy value is varying between 90.3% to 94.4%, which is achieved at $p \leq 0.01$. In multiclass classification, shown in Table 5, NOC achieved the highest accuracy at $p \leq 0.1$, giving 88.9% whereas PCC obtained the highest accuracy at $p \leq 0.07$. It is clear from the result in Table 4 and 5, that NOC performed better than PCC in classifying ASD subtypes against the NC.

In the subsequent sections, Section IV-B and IV-C, respectively, multiclass and 2-class ASD subtypes (ATD/APD/PDD vs. NC) performance evaluation result for classification will be presented using the number of S as shown in Figure 3 that gives the best accuracy. Specifically, for 2-class, the NOC will use S obtained at $p \leq 0.1$, whereas, PCC will use S obtained at $p \leq 0.01$. For multiclass, NOC will use S obtained at $p \leq 0.1$ and PCC will use S obtained at $p \leq 0.07$. Since the dataset of multiclass ASD is relatively small, we further validate our proposed classification framework in Section IV-D using a larger dataset from ABIDE having 505-ASD and 530-NC subjects.

B. MULTICLASS CLASSIFICATION OF ASD SUBTYPES AND NORMAL CONTROL

In this section, the performance of the NOC-based ML algorithm is evaluated for multiclass detection of ASD subtypes (ATD, APD, PDD) and NC. The evaluation is presented in terms of macro accuracy obtained using a 5-fold and 10-fold CV framework. At the beginning of the experiment, many classifiers are tested but only the top 3 classifiers are selected to be presented in this section. The shortlisted classifiers are cubic SVM, cosine KNN, and ensemble subspace discriminant where the parameters for each classifier are specified as in Section III-E. In essence, this experiment is used to determine the best ML classifier in discriminating the ASD subtypes and NC subjects. The accuracy values for 3 best ML classifiers are evaluated by using 1816-PCC and 984-NOC most significant connections as given in Figure 3. Only the top-selected features from a total of 6670 features are used as feature vectors to the ML classifiers.

From Table 6 classification based on NOC feature outperformed the PCC feature with the best accuracy of 88.9 % and 87.08 %, for 10-fold and 5-fold, respectively. Relative to the PCC-based approach, the NOC-based approach obtained

TABLE 4. Two-class classification accuracy (in %) for 3 ASD subtypes versus NC evaluated at different p values using cubic SVM and 10-fold CV. The number of connections of NOC and PCC for each p-value are as shown in Figure 3(a)-(b). There are 36 subjects for each ASD subtypes and NC.

Method	Class	0.01	0.03	0.05	0.07	0.09	0.1
NOC	ATD vs. NC	93.62 ±0.63	97.18 ±0.5	**98.6** ±0.62	97.9 ±0.7	95.4 ±1.6	95.53 ±1.72
	APD vs. NC	96.64 ±0.92	96.78 ±0.89	**97.2** ±0.88	96.64 ±1.12	96.37 ±1.66	95.94 ±1.7
	PDD vs. NC	95.13 ±1.52	96.78 ±1.26	**97.2** ±0.08	96.92 ±1.04	96.78 ±1.09	95.54 ±2.03
PCC	ATD vs. NC	**94.4** ±1.2	92.24 ±1.65	90.86 ±0.68	91.42 ±1.37	89.74 ±1.89	90.86 ±1.42
	APD vs. NC	**90.3** ±1.85	90.02 ±1.22	89.88 ±1.98	87.64 ±1.16	88.34 ±0.92	87.64 ±0.98
	PDD vs. NC	**94.4** ±1.2	93.49 ±0.59	91.55 ±1.44	89.74 ±1.89	90.15 ±2.36	91.39 ±2.37

TABLE 5. Multiclass classification accuracy (in %) for 3 ASD subtypes and NC, evaluated at different p values using cubic SVM and 10-fold CV. The number of connections of NOC and PCC for each p-value are as shown in Figure 3(c).

Method	0.01	0.03	0.05	0.07	0.09	0.1
NOC	70.76 ±1.85	82.55 ±1.93	85.61 ±1.65	84.56 ±1.28	87.15 ±1.22	**88.9** ±0.85
PCC	73.53 ±1.64	77.17 ±0.96	75.28 ±1.29	**79.94** ±1.51	75.28 ±0.94	75.35 ±0.35

TABLE 6. Macro-accuracy (in %) expressed with standard deviation (.) of multiclass ASD classification using 1816-PCC and 984-NOC significant connections obtained at $p \leq 0.07$ and $p \leq 0.1$ for PCC and NOC, respectively. The 3 classifiers used in this case are cubic SVM, cosine KNN and ensemble subspace discriminant (EnSub), evaluated using 5-fold and 10-fold CV.

Classifier	5-Fold		10-Fold	
	PCC	NOC	PCC	NOC
SVM	76.68(1.57)	87.08(1.6)	79.94(1.5)	88.97(0.85)
KNN	61.52(2.15)	76.12(1.5)	60.54(3.23)	78.08(1.63)
EnSub	55.14(2.43)	61.8(3.31)	58.26(2.86)	60.97(3.17)

TABLE 7. Macro (Acc, Sen, Spe, Pre) performance of 10-fold multiclass classification of ATD, APD, and PDD vs. NC using 1816-PCC and 984-NOC significant connections obtained at $p \leq 0.07$ and $p \leq 0.1$ for PCC and NOC, respectively. The result is generated using cubic SVM.

Metric (%)	ATD		APD		PDD		NC	
	PCC	NOC	PCC	NOC	PCC	NOC	PCC	NOC
Acc	88.88	92.36	92.36	94.44	88.88	95.13	89.58	95.83
Sen	71.7	79.06	90.32	93.75	79.41	91.42	81.8	94.11
Spe	96.93	98.01	92.9	94.64	91.81	96.33	91.89	96.36
Pre	91.66	94.4	77.77	83.33	75	88.88	75	88.88

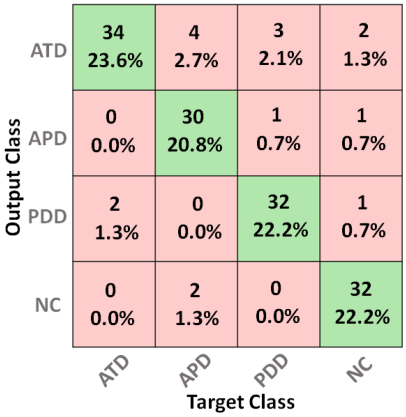

FIGURE 4. Confusion matrix for multiclass classification of ASD subtypes using NOC and cubic SVM.

10.4 % and 9.03 % higher accuracy for 5-fold and 10-fold CV, respectively. Performance based on PCC hardly reaches 80% and the best result is 79.94% obtained using SVM. From the result of this section, it is clear that cubic SVM gives the best performance in terms of accuracy and therefore will be selected as the classifier for the next experiments.

A more detailed assessment on the NOC-based multiclass classification is conducted using 10-fold CV and the result of accuracy, sensitivity, specificity, and precision is provided in Table 7. The values in Table 7 are calculated from the confusion matrix in Figure 4. In general, a clear trend shows that NOC-based classification performed better than the PCC. The average accuracy of NOC-based classification across all 4 classes is at 94.44% which is 4.5% higher than the PCC. Better sensitivity by the NOC is recorded at an average value of 89.5% which is 8.69% higher than the PCC. The measure of how well the classification method detects true negative cases, is provided by the specificity. For NOC and PCC, the average specificity is at 96.33% and 93.37%, only differed by 2.96%. Lastly, the average precision is recorded at 88.8% for NOC compared to 79.85% for PCC indicating that NOC is 8.9% better than the PCC.

For comparison with the recent work on multiclass ASD classification, we considered the work by Hiyali *et al.* [22]. In [22], the multiclass classification used dynamic FC patterns in the form of wavelet coherence scalograms, representing the phase synchronization between the pairs of BOLD signals. Using a 3-layer CNN architecture taking wavelet coherence scalograms of 116 brain regions as its input, the method in [22] achieved the best accuracy of 82.1%. In comparison to the proposed NOC-based multiclass classification as shown in Table 6, with the best macro-accuracy of 88.97%, the NOC outperformed the wavelet coherence technique [22] by 6.87%.

C. 2-CLASS CLASSIFICATION OF ASD SUBTYPES VS. NORMAL CONTROL USING CUBIC SVM

Apart from multiclass classification, the accuracy of the classification algorithm employing NOC and cubic SVM for 2-class classification of ASD subtypes versus NC is evaluated. The results of 2-class ASD subtypes classification are given in Table 4, utilizing a 10-fold CV framework. The best

results are highlighted in bold-font, with S set at 0.05 and 0.01 for NOC and PCC, respectively.

Clearly, results of NOC-based classification indicate its excellent performance over the PCC approach. With accuracy of 98.6% for ATD vs. NC and 97.2% across other two 2-class cases, this value is 4.2, 6.9% and 2.8% higher than the PCC approach. In addition, the notable performance of NOC-based is also evident from its perfect sensitivity and 97.1% score for specificity and precision as well as almost 100% AUC. Besides, relative to PCC-based, the NOC exhibits low standard deviation (<1%) as detailed in Table 4 which indicates good generalization of the classification model across different training sets. However, since the dataset of 72-subject is relatively small, further investigation of ASD vs. NC is conducted using 1035-subject dataset and presented the next Section IV-D.

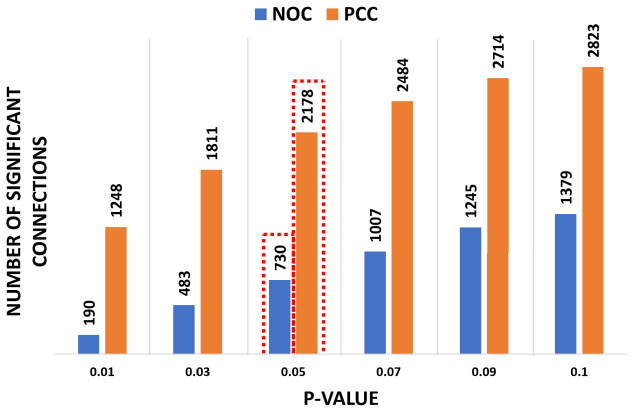

FIGURE 5. Significant connections of 2-class NOC and PCC binary classification, extracted at different p values using the 1035-subject dataset. The significant connections that result in the best performance for NOC and PCC as determined from Table 8 are highlighted in a red dashed-box.

D. PERFORMANCE OF NOC-BASED BINARY CLASSIFICATION OF ASD VERSUS NC USING 1035-SUBJECT DATASET

In this section, the proposed method is evaluated using the full ABIDE dataset having 505 ASD subjects and 530 NC subjects. Unlike the ASD subtypes cases presented in Section IV-B and IV-C, since the dataset is small, only CV framework is utilized in its evaluation.

Here, the data is split into training and testing taking 90% data for training using 10-fold CV and 10% data for testing from each class. This test data is unseen by the train/validation procedure used in model training. The p-value analysis is conducted for the selection of top-ranked features. Table 8 shows the classification accuracy for ASD vs. NC classification, evaluated at different p values ranging from 0.01-0.1 using Gaussian SVM and 10-fold CV framework. From Table 8, it can be seen that the highest testing accuracy achieved at $p \leq 0.05$ which is 80% and 68% for NOC and PCC, respectively. Notably, the proposed method outperformed the conventional PCC approach by 12% in terms of accuracy on a larger dataset.

For the detailed evaluation at $p \leq 0.05$, the performance metric such as accuracy, sensitivity, specificity and precision are calculated for the NOC and PCC approaches, using the 10% test data. These values are listed in the confusion matrix as given in Figure 6. The proposed NOC-based method maintained a good balance between sensitivity and specificity of 80% for NOC while it is at 68% and 58% for PCC, respectively. Similarly, the NOC approach obtained 7.5% more precise in its decision compared to the PCC approach which is at 72.5% precision.

For the past couple of years, there have been numerous attempts in finding biomarkers that can automatically diagnose ASD using fMRI signals. The list of the state-of-the-art techniques in comparison to the NOC-based method is tabulated in Table 9. Generally, the methods differ in terms of the brain's ROI, feature extraction and type of classifiers. Clearly, utilizing small ROI, 36 [24] and 160 [23] will not provide better classification results than the NOC-based method. It can also be seen that the type of feature plays a significant role in determining the classification results. Pearson correlation at ROI of 116 [27] or greater [25], [26], [28] is only able to reach the best accuracy of 74% using SVM [27]. The work by Heinsfeld *et al.* [25], Eslami *et al.* [26], Tang *et al.* [27] and Huang *et al.* [29] provide a fair comparison to our proposed method since they all used the same dataset.

One recent paper on fMRI-based diagnosis of autism using the ABIDE dataset is by Yang *et al.* [54] which is based on Pearson's correlation-based spatial constraints representation (PSCR) and graph attention network (GAT) framework. Their proposed method achieved 72.4% accuracy, which is less accurate than our NOC-based method. Comparison with the most recent state-of-the-art techniques by Huang *et al.* [29] and Yang *et al.* [54], shows that our method based on NOC has outperformed [29] and [54], respectively, by 3.6% and 7.6% in terms of classification accuracy. With this result, it is clear that the proposed method in this study provides a more reliable result for automatic diagnosis of ASD.

E. ANALYSIS ON SIGNIFICANT PAIRS OF BRAIN CONNECTIONS

In this section, We select the top twenty significant pairs of connections out of 6670 connections based on p-value analysis. The list of 20 pairs of node connection and its class of function, i.e. whether a particular node is linked to primary, association or also known as secondary, paralimbic and subcortical functionality is given in Table 10. The plot of the nodes on the left and right hemisphere of the brain is shown in Figure 7. From the four brain functionalities, 12 nodes are from association function, followed by 5 nodes from both paralimbic and subcortical and lastly, 2 nodes from primary function. This result indicates that the secondary or association region is highly affected by the ASD condition. This can be attributed to the important role of the association

TABLE 8. Classification accuracy (in %) for ASD vs NC classification using 1035-subject dataset, evaluated at different p values using Gaussian SVM and 10-fold CV. The number of connections of NOC and PCC for each p-value are shown in Figure 5.

Method	0.01		0.03		0.05		0.07		0.09		0.1	
	CV	Test	CV	Test	CV	Test	CV	Test	CV	Test	CV	Test
NOC	73.12 ±0.002	79	70.4 ±0.002	70	75.83 ±0.009	**80**	74.79 ±0.007	75	74.7 ±0.005	74	72.3 ±0.004	75
PCC	70.2 ±0.009	63	70 ±0.009	65	70 ±0.004	**68**	71.4 ±0.004	64	70.2 ±0.009	63	71.4 ±0.007	60

TABLE 9. ASD vs. NC classification comparison with previous studies in terms of accuracy, sensitivity, specificity (in %) and AUC.

Method	Region of Interest (ROI)	Feature Set	Classifier	Subjects		Evaluation Metric			
				NC	ASD	Acc	Sen	Spe	AUC
Chen et al. (2016) [23]	Dosenbach 160	Pearson correlation	SVM	128	112	79.17	77.78	80.47	0.856
Abraham et al. (2017) [24]	MSDL 39	Covariance estimation	SVM	468	403	67	90.9	61.3	-
Heinsfeld et al. (2018) [25]	CC200	Pearson correlation	DNN	530	505	70	74	63	-
Eslami et al. (2019) [26]	CC200	Pearson correlation	autoencoder+SLP	530	505	70.3	68.3	72.2	-
Tang et al. (2020) [27]	AAL 116	Pearson correlation	SVM	530	505	74	-	-	-
Sherkatghanad et al. (2020) [28]	CC400	Pearson correlation	CNN	573	539	70.22	77.46	61.82	0.74
Huang et al. (2021) [29]	CC200	Graph theory	CNN	530	505	76.4	77.8	75	0.75
Yang et al. (2021) [54]	HO110	PSCR	GAT	468	403	72.4	71.15	75	0.758
Ours	**AAL 116**	**Non-oscillatory connectivity**	**SVM**	**530**	**505**	**80**	**80**	**80**	**0.8**

TABLE 10. The top twenty significant pairs of brain node connections with its type of function. The number in bracket after abbreviation denotes the node number as per AAL-116 atlas.

	Class	Node Name	Node Abbreviation	Link	Class	Node Name	Node Abbreviation
1	Association	Superior frontal gyrus, dorsolateral	SFGdor.R(4)	⟷	Association	Angular gyrus	ANG.L(65)
2	Association	Inferior frontal gyrus, triangular	IFGtriang.R(14)	⟷	Paralimbic	Cingulate gyrus, anterior part	ACG.L(31)
3	Association	Inferior frontal gyrus, triangular	IFGtriang.R(14)	⟷	Paralimbic	Superior frontal gyrus, medial orbital	REC.R(28)
4	Paralimbic	Inferior frontal gyrus, orbital	ORBinf.R(16)	⟷	Paralimbic	Gyrus rectus	ORBsupmed.R(26)
5	Paralimbic	Inferior frontal gyrus, orbital	ORBinf.R(16)	⟷	Paralimbic	Gyrus rectus	REC.R(28)
6	Association	Superior frontal gyrus, medial	SFGmed.R(24)	⟷	Association	Angular gyrus	ANG.L(65)
7	Association	Superior frontal gyrus, medial orbital	ORBsupmed.L(25)	⟷	Association	Precuneus	PCUN.R(68)
8	Association	Superior frontal gyrus, medial orbital	ORBsupmed.R(26)	⟷	Subcortical	Vermis 4 5	Vermis45(111)
9	Paralimbic	Gyrus rectus	REC.R(28)	⟷	Paralimbic	Cingulate gyurs, posterior part	PCG.L(35)
10	Paralimbic	Gyrus rectus	REC.R(28)	⟷	Association	Precuneus	PCUN.R(68)
11	Paralimbic	Gyrus rectus	REC.R(28)	⟷	Subcortical	Vermis 4 5	Vermis45(111)
12	Subcortical	Hippocampus	HIP.R(38)	⟷	Association	Middle temporal gyrus	MTG.R(86)
13	Association	Cuneus	CUN.L(45)	⟷	Association	Middle temporal gyrus	MTG.R(86)
14	Primary	Postcentral gyrus	PoCG.R(58)	⟷	Subcortical	Cerebellum crus 2	CRBLCrus2.L(93)
15	Association	Inferior parietal gyrus	IPL.L(61)	⟷	Association	Precuneus	PCUN.R(68)
16	Subcortical	Thalamus	THA.L(77)	⟷	Association	Middle temporal gyrus	MTG.L(85)
17	Subcortical	Thalamus	THA.L(77)	⟷	Primary	Heschl gyrus	HES.L(79)
18	Subcortical	Thalamus	THA.R(78)	⟷	Association	Superior temporal gyrus	STG.R(82)
19	Subcortical	Thalamus	THA.R(78)	⟷	Association	Middle temporal gyrus	MTG.L(85)
20	Subcortical	Thalamus	THA.R(78)	⟷	Association	Middle temporal gyrus	MTG.R(86)

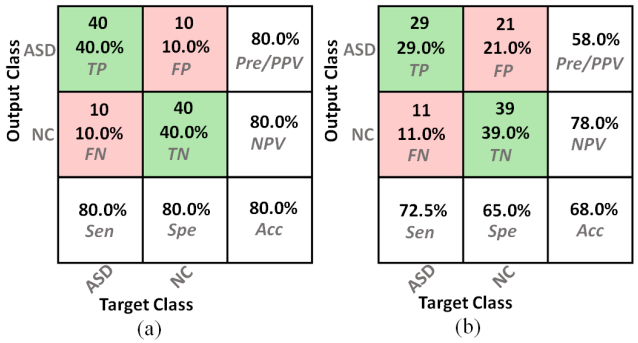

FIGURE 6. Confusion matrix for 2-class classification of 50 AD and 50 NC test subjects from 1035-subject dataset, based on (a) NOC and (b) PCC using Gaussian SVM. Testing of the model is performed using significant connections, S at $p \leq 0.05$ for NOC and PCC, with S respectively, equal to 730 and 2178 as determined from Figure 5. Here, PPV is positive predictive rate which is also known as precision and NPV is negative predictive rate.

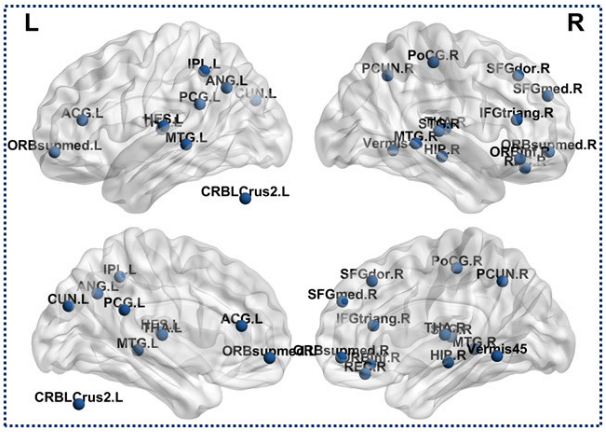

FIGURE 7. Significant nodes of 20 most significant connection pairs as listed in Table 10.

areas which is to integrate incoming sensory information, and also form connections between sensory and motor areas for the primary area. For further validation, we compare our nodes with the findings by C Y Wee *et al.* [55], who proposed a framework using short-time activation patterns of brain connectivity from resting-state fMRI in diagnosis of ASD. Notably, the nodes, including inferior frontal gyrus triangular, hippocampus, inferior parietal gyrus, middle temporal gyrus

listed in Table 10 matched the findings in [55]. In fact, the 14 discriminative nodes listed in [55] matched with the nodes of our 730 significant connections, obtained based on *p*-value analysis.

V. LIMITATIONS, CHALLENGES AND FUTURE WORK

Although the NOC-based classification has shown to be a promising fMRI feature for classification of ASD, there remain limitations in the current study that could be addressed by future work. Firstly, a single large publicly available fMRI dataset of multiclass ASD is not readily available, hence data across multiple sites with different acquisition protocols need to be considered in the future. With the dataset of 36 subjects per class, this number is considered to be relatively small. Hence, before being used in clinical trials, the proposed technique should be trained and evaluated on a larger number of subjects, to be obtained across multiple sites. Secondly, other than *p*-value analysis other feature selection techniques, such as ReliefF and mRMR can be investigated which may improve the accuracy, especially for multiclass classification.

Lastly, with accuracy of 88.9% and 80%, respectively, for multiclass and binary classification, there is room for improvement for the NOC-based classification of ASD subtypes. This can be explored by using brain atlas with higher number of regions. For example, Craddock CC200/CC400, which defined 200/400 brain regions may provide better representation on the brain's neural activity, in turn giving better classification of ASD subtypes.

Future work on the NOC-based technique may include diagnosis of other brain disorders such as alcohol use disorder, major depressive disorder, schizophrenia, and early Alzheimer detection, etc. Besides, more detailed analysis of affected brain regions and its functionality related to the ASD, as identified by the NOC should also be conducted. This may lead to important findings on NOC-based biomarkers for diagnosis of not only ASD but various brain disorders and provide interpretability of the machine learning model.

VI. CONCLUSION

In this paper, a classification algorithm for detecting 3 autism subtypes and normal control is developed using the non-oscillatory connectivity (NOC) approach. The non-oscillatory connectivity provides pure neuronal activity free from the influences of the oscillatory components emanating from sources like cardiac and respiratory systems. The NOC-based approach showed excellent performance in classifying ATD vs. NC, APD vs. NC, PDD vs. NC and multiclass classification. In fact, its 2-class classification outperformed the Pearson correlation based approach by a margin of 5.65% to 7.74% and the recently published work by 12.7%. The excellent performance of the NOC-based approach may be attributed to better neural representation by the NOC, hence giving a positive impact in the classification of the ASD subtypes. It should be noted that the performance evaluation of the proposed approach is obtained based on 36 subjects per class, which is a relatively small sample size. Therefore, a larger dataset consisting of 1035 subjects is also included to evaluate the performance of the proposed method that achieved the classification accuracy of 80% which is 12% more compared to PCC approach which is at 68%. The proposed method also outperformed the recently developed approaches by a good margin as summarized in Table 9.

REFERENCES

[1] J. Baio *et al.*, "Prevalence of autism spectrum disorder among children aged 8 years—Autism and developmental disabilities monitoring network, 11 sites, United States, 2014," *Morbidity Mortality Weekly Rep. Surveill. Summaries*, vol. 67, pp. 1–23, Apr. 2018.

[2] M. Elsabbagh, G. Divan, Y.-J. Koh, Y. S. Kim, S. Kauchali, C. Marcín, C. Montiel-Nava, V. Patel, C. S. Paula, C. Wang, M. T. Yasamy, and E. Fombonne, "Global prevalence of autism and other pervasive developmental disorders," *Autism Res., Off. J. Int. Soc. Autism Res.*, vol. 5, no. 3, pp. 160–179, Jun. 2012.

[3] *Diagnostic and Statistical Manual of Mental Disorders (DSM–5)*, 5th ed., Amer. Psychiatric Assoc., Washington, DC, USA, 2013.

[4] V. Y. Tittagalla, R. R. P. Wickramarachchi, G. W. C. N. Chandrarathne, N. M. D. M. B. Nanayakkara, P. Samarasinghe, P. Rathnayake, and M. G. N. M. Pemadasa, "Screening tool for autistic children," in *Proc. 11th Int. Conf. Knowl. Smart Technol. (KST)*, Jan. 2019, pp. 132–136.

[5] F. R. Volkmar, "Editorial: The importance of early intervention," *J. Autism Develop. Disorders*, vol. 44, no. 12, pp. 2979–2980, Dec. 2014.

[6] D. A. Rotholz, A. M. Kinsman, K. K. Lacy, and J. Charles, "Improving early identification and intervention for children at risk for autism spectrum disorder," *Pediatrics*, vol. 139, no. 2, pp. 1–7, Feb. 2017.

[7] A. R. Swanson, Z. E. Warren, W. L. Stone, A. C. Vehorn, E. Dohrmann, and Q. Humberd, "The diagnosis of autism in community pediatric settings: Does advanced training facilitate practice change?" *Autism*, vol. 18, no. 5, pp. 555–561, Jul. 2014.

[8] (2020). *Screening and Diagnosis of Autism Spectrum Disorder*. [Online]. Available: https://www.cdc.gov/ncbddd/autism/screening.html

[9] R. M. Jones and C. Lord, "Diagnosing autism in neurobiological research studies," *Behav. Brain Res.*, vol. 251, pp. 113–124, Aug. 2013.

[10] B. B. Maddox, E. S. Brodkin, M. E. Calkins, K. Shea, K. Mullan, J. Hostager, D. S. Mandell, and J. S. Miller, "The accuracy of the ADOS-2 in identifying autism among adults with complex psychiatric conditions," *J. Autism Develop. Disorders*, vol. 47, no. 9, pp. 2703–2709, Sep. 2017.

[11] J. A. Reaven, S. L. Hepburn, and R. G. Ross, "Use of the ADOS and ADI-R in children with psychosis: Importance of clinical judgment," *Clin. Child Psychol. Psychiatry*, vol. 13, no. 1, pp. 81–94, Jan. 2008.

[12] R. Grzadzinski, C. Dick, C. Lord, and S. Bishop, "Parent-reported and clinician-observed autism spectrum disorder (ASD) symptoms in children with attention deficit/hyperactivity disorder (ADHD): Implications for practice under DSM-5," *Mol. Autism*, vol. 7, no. 1, Jan. 2016, Art. no. 7.

[13] A. Abi-Dargham and G. Horga, "The search for imaging biomarkers in psychiatric disorders," *Nature Med.*, vol. 22, no. 11, pp. 1248–1255, Nov. 2016.

[14] Š. Holiga *et al.*, "Patients with autism spectrum disorders display reproducible functional connectivity alterations," *Sci. Transl. Med.*, vol. 11, no. 481, p. eaat9223, 2019. [Online]. Available: https://www.science.org/doi/abs/10.1126/scitranslmed.aat9223, doi: 10.1126/scitranslmed.aat9223.

[15] S. Xu, M. Li, C. Yang, X. Fang, M. Ye, L. Wei, J. Liu, B. Li, Y. Gan, B. Yang, W. Huang, P. Li, X. Meng, Y. Wu, and G. Jiang, "Altered functional connectivity in children with low-function autism spectrum disorders," *Frontiers Neurosci.*, vol. 13, p. 806, Aug. 2019.

[16] S. Yao, B. Becker, and K. M. Kendrick, "Reduced inter-hemispheric resting state functional connectivity and its association with social deficits in autism," *Frontiers Psychiatry*, vol. 12, p. 244, Mar. 2021.

[17] A. D. Savva, A. S. Karampasi, and G. K. Matsopoulos, "Deriving resting-state fMRI biomarkers for classification of autism spectrum disorder," in *Autism 360°*, U. Das, N. Papaneophytou, and T. El-Kour, Eds. New York, NY, USA: Academic, 2020, ch. 6, pp. 101–123.

[18] R. M. Thomas, S. Gallo, L. Cerliani, P. Zhutovsky, A. El-Gazzar, and G. van Wingen, "Classifying autism spectrum disorder using the temporal statistics of resting-state functional MRI data with 3D convolutional neural networks," *Frontiers Psychiatry*, vol. 11, p. 440, May 2020.

[19] A. M. DSouza, A. Z. Abidin, and A. Wismüller, "Classification of autism spectrum disorder from resting-state fMRI with mutual connectivity analysis," *Proc. SPIE*, vol. 10953, pp. 292–299, Mar. 2019.
[20] A. Bernas, A. P. Aldenkamp, and S. Zinger, "Wavelet coherence-based classifier: A resting-state functional MRI study on neurodynamics in adolescents with high-functioning autism," *Comput. Methods Programs Biomed.*, vol. 154, pp. 143–151, Feb. 2018.
[21] M. I. Al-Hiyali, N. Yahya, I. Faye, and Z. Khan, "Autism spectrum disorder detection based on wavelet transform of BOLD fMRI signals using pre-trained convolution neural network," *Int. J. Integr. Eng.*, vol. 13, no. 5, pp. 49–56, May 2021.
[22] M. I. Al-Hiyali, N. Yahya, I. Faye, and A. F. Hussein, "Identification of autism subtypes based on wavelet coherence of BOLD FMRI signals using convolutional neural network," *Sensors*, vol. 21, no. 16, p. 5256, Aug. 2021.
[23] H. Chen, X. Duan, F. Liu, F. Lu, X. Ma, Y. Zhang, L. Q. Uddin, and H. Chen, "Multivariate classification of autism spectrum disorder using frequency-specific resting-state functional connectivity—A multi-center study," *Prog. Neuro-Psychopharmacol. Biol. Psychiatry*, vol. 64, pp. 1–9, Jan. 2016.
[24] A. Abraham, M. P. Milham, A. Di Martino, R. C. Craddock, D. Samaras, B. Thirion, and G. Varoquaux, "Deriving reproducible biomarkers from multi-site resting-state data: An autism-based example," *NeuroImage*, vol. 147, pp. 736–745, Feb. 2017.
[25] A. S. Heinsfeld, A. R. Franco, R. C. Craddock, A. Buchweitz, and F. Meneguzzi, "Identification of autism spectrum disorder using deep learning and the ABIDE dataset," *NeuroImage, Clin.*, vol. 17, pp. 16–23, Jan. 2018.
[26] T. Eslami, V. Mirjalili, A. Fong, A. R. Laird, and F. Saeed, "ASD-DiagNet: A hybrid learning approach for detection of autism spectrum disorder using fMRI data," *Frontiers Neuroinform.*, vol. 13, p. 70, Nov. 2019.
[27] M. Tang, P. Kumar, H. Chen, and A. Shrivastava, "Deep multimodal learning for the diagnosis of autism spectrum disorder," *J. Imag.*, vol. 6, no. 6, p. 47, Jun. 2020.
[28] Z. Sherkatghanad, M. Akhondzadeh, S. Salari, M. Zomorodi-Moghadam, M. Abdar, U. R. Acharya, R. Khosrowabadi, and V. Salari, "Automated detection of autism spectrum disorder using a convolutional neural network," *Frontiers Neurosci.*, vol. 13, p. 1325, Jan. 2020.
[29] Z.-A. Huang, Z. Zhu, C. H. Yau, and K. C. Tan, "Identifying autism spectrum disorder from resting-state fMRI using deep belief network," *IEEE Trans. Neural Netw. Learn. Syst.*, vol. 32, no. 7, pp. 2847–2861, Jul. 2021.
[30] N. Chaitra, P. A. Vijaya, and G. Deshpande, "Diagnostic prediction of autism spectrum disorder using complex network measures in a machine learning framework," *Biomed. Signal Process. Control*, vol. 62, Sep. 2020, Art. no. 102099.
[31] D. M. Khan, N. Yahya, N. Kamel, and I. Faye, "Automated diagnosis of major depressive disorder using brain effective connectivity and 3D convolutional neural network," *IEEE Access*, vol. 9, pp. 8835–8846, 2021.
[32] D. M. Khan, N. Yahya, N. Kamel, and I. Faye, "Effective connectivity in default mode network for alcoholism diagnosis," *IEEE Trans. Neural Syst. Rehabil. Eng.*, vol. 29, pp. 796–808, 2021.
[33] Y. Kong, J. Gao, Y. Xu, Y. Pan, J. Wang, and J. Liu, "Classification of autism spectrum disorder by combining brain connectivity and deep neural network classifier," *Neurocomputing*, vol. 324, pp. 63–68, Jan. 2019.
[34] D. M. Khan, N. Kamel, M. Muzaimi, and T. Hill, "Effective connectivity for default mode network analysis of alcoholism," *Brain Connectivity*, vol. 11, no. 1, pp. 12–29, Feb. 2021.
[35] Y. Ikeda, M. Kikuchi, M. Noguchi-Shinohara, K. Iwasa, M. Kameya, T. Hirosawa, M. Yoshita, K. Ono, M. Samuraki-Yokohama, and M. Yamada, "Spontaneous MEG activity of the cerebral cortex during eyes closed and open discriminates Alzheimer's disease from cognitively normal older adults," *Sci. Rep.*, vol. 10, no. 1, p. 9132, Jun. 2020.
[36] X. Zhang, C.-Q. Chen, M.-K. Zhang, C.-Y. Ma, Y. Zhang, H. Wang, Q.-Q. Guo, T. Hu, Z.-B. Liu, Y. Chang, K.-J. Hu, and X.-D. Yang, "Detection and analysis of MEG signals in occipital region with double-channel OPM sensors," *J. Neurosci. Methods*, vol. 346, Dec. 2020, Art. no. 108948.
[37] W. You, S. Achard, J. Stadler, B. Brückner, and U. Seiffert, "Fractal analysis of resting state functional connectivity of the brain," in *Proc. Int. Joint Conf. Neural Netw. (IJCNN)*, Jun. 2012, pp. 1–8.
[38] V. Maxim, L. Şendur, J. Fadili, J. Suckling, R. Gould, R. Howard, and E. Bullmore, "Fractional Gaussian noise, functional MRI and Alzheimer's disease," *NeuroImage*, vol. 25, no. 1, pp. 141–158, Mar. 2005.
[39] E. Zarahn, G. K. Aguirre, and M. D'Esposito, "Empirical analyses of BOLD fMRI statistics," *NeuroImage*, vol. 5, no. 3, pp. 179–197, Apr. 1997.
[40] C. J. Stam and E. A. de Bruin, "Scale-free dynamics of global functional connectivity in the human brain," *Hum. Brain Mapping*, vol. 22, no. 2, pp. 97–109, Jun. 2004.
[41] D. Van De Ville, J. Britz, and C. M. Michel, "EEG microstate sequences in healthy humans at rest reveal scale-free dynamics," *Proc. Nat. Acad. Sci. USA*, vol. 107, no. 42, pp. 18179–18184, Oct. 2010.
[42] P. Expert, R. Lambiotte, D. R. Chialvo, K. Christensen, H. J. Jensen, D. J. Sharp, and F. Turkheimer, "Self-similar correlation function in brain resting-state functional magnetic resonance imaging," *J. Roy. Soc. Interface*, vol. 8, no. 57, pp. 472–479, Apr. 2011.
[43] B. J. West, R. Zhang, A. W. Sanders, S. Miniyar, J. H. Zuckerman, and B. D. Levine, "Fractal fluctuations in cardiac time series," *Phys. A, Stat. Mech. Appl.*, vol. 270, nos. 3–4, pp. 552–566, Aug. 1999.
[44] R. M. Birn, J. B. Diamond, M. A. Smith, and P. A. Bandettini, "Separating respiratory-variation-related fluctuations from neuronal-activity-related fluctuations in fMRI," *NeuroImage*, vol. 31, no. 4, pp. 1536–1548, Jul. 2006.
[45] S. Achard, D. S. Bassett, A. Meyer-Lindenberg, and E. Bullmore, "Fractal connectivity of long-memory networks," *Phys. Rev. E, Covering Stat., Nonlinear, Biol., Soft Matter Phys.*, vol. 77, no. 3, Mar. 2008, Art. no. 036104.
[46] M. Clausel, F. Roueff, M. S. Taqqu, and C. Tudor, "Large scale behavior of wavelet coefficients of non-linear subordinated processes with long memory," *Appl. Comput. Harmon. Anal.*, vol. 32, no. 2, pp. 223–241, Mar. 2012.
[47] J. Nielsen, B. Zielinski, P. Fletcher, A. Alexander, N. Lange, E. Bigler, J. Lainhart, and J. Anderson, "Multisite functional connectivity MRI classification of autism: ABIDE results," *Frontiers Hum. Neurosci.*, vol. 7, 2013. [Online]. Available: https://www.frontiersin.org/article/10.3389/fnhum.2013.00599, doi: 10.3389/fnhum.2013.00599.
[48] S. Whitfield-Gabrieli and A. Nieto-Castanon, "Conn: A functional connectivity toolbox for correlated and anticorrelated brain networks," *Brain Connectivity*, vol. 2, no. 3, pp. 125–141, Jun. 2012.
[49] C. G. Yan, X. D. Wang, X. N. Zuo, and Y. F. Zang, "DPABI: Data processing & analysis for (resting-state) brain imaging," *Neuroinformatics*, vol. 14, no. 3, pp. 339–351, Apr. 2016.
[50] N. Tzourio-Mazoyer, B. Landeau, D. Papathanassiou, F. Crivello, O. Etard, N. Delcroix, B. Mazoyer, and M. Joliot, "Automated anatomical labeling of activations in SPM using a macroscopic anatomical parcellation of the MNI MRI single-subject brain," *NeuroImage*, vol. 15, no. 1, pp. 273–289, Jan. 2002.
[51] L. Chen, C. Rong, and J. Feng, "Time series join on most correlated subsequences using MapReduce," in *Proc. IEEE 21st Int. Conf. High Perform. Comput. Commun., IEEE 17th Int. Conf. Smart City, IEEE 5th Int. Conf. Data Sci. Syst. (HPCC/SmartCity/DSS)*, Aug. 2019, pp. 1366–1373.
[52] M. Döring. (Dec. 2018). *Performance Measures for Multi-Class Problems*. [Online]. Available: https://www.datascienceblog.net/post/machine-learning/performance-measures-multi-class-problems/
[53] K. Friston, J. Ashburner, S. Kiebel, T. Nichols, and W. Penny, Eds., "Acknowledgements," in *Statistical Parametric Mapping*. London, U.K.: Academic, 2007, p. 7.
[54] C. Yang, P. Wang, J. Tan, Q. Liu, and X. Li, "Autism spectrum disorder diagnosis using graph attention network based on spatial-constrained sparse functional brain networks," *Comput. Biol. Med.*, vol. 139, Dec. 2021, Art. no. 104963.
[55] C.-Y. Wee, P.-T. Yap, and D. Shen, "Diagnosis of autism spectrum disorders using temporally distinct resting-state functional connectivity networks," *CNS Neurosci. Therapeutics*, vol. 22, no. 3, pp. 212–219, 2016.

ALISHBA SADIQ received the B.E. and M.S. degrees in electronics engineering from the Pakistan Air-Force Karachi Institute of Economics and Technology (PAF-KIET), Pakistan, in 2015 and 2018, respectively. She is currently pursuing the Ph.D. degree with Universiti Teknologi PETRONAS, Malaysia. In 2016, she joined PAF-KIET as a Graduate Teaching Fellow (GTF). Since 2016, she has been associated with the Signal Processing Research Group (SPRG) as a Research Assistant. She is currently a Research Graduate Assistant at the Center for Intelligent Signal and Imaging Research (CISIR), Universiti Teknologi PETRONAS. Her research interests include machine learning, pattern classification, biomedical image analysis, neurological disorder's diagnosis, and brain connectivity.

MOHAMMED ISAM AL-HIYALI received the B.Eng. degree in laser and optoelectronics engineering from Al-Nahrain University, Iraq, in 2010, and the master's degree in biomedical engineering from Universiti Putra Malaysia (UPM), Malaysia, in 2019. He is currently pursuing the Ph.D. degree with Universiti Teknologi PETRONAS (UTP), Malaysia. His research interests include artificial intelligence, image and signal processing, medical imaging, and deep learning.

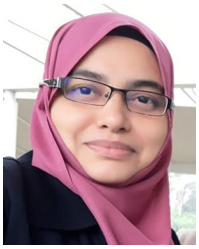

NORASHIKIN YAHYA received the B.Eng. degree (Hons.) in electronic engineering from the University of Sheffield, U.K., in 2001, the M.Sc. degree in electrical engineering from Lehigh University, USA, in 2004, and the Ph.D. degree in electrical engineering from Universiti Teknologi PETRONAS (UTP), Malaysia, in 2015. She is currently a Senior Lecturer at UTP and also a member of the Centre for Intelligent Signal and Imaging Research (CISIR) Laboratory, one of the National Higher Institution Centre of Excellence (HICoE) status focusing on neuro signal and image analysis as its research niche area. Her research interests include image segmentation and pattern recognition involving biomedical signals and images using machine learning and deep learning techniques.

TONG BOON TANG (Senior Member, IEEE) received the B.Eng. (Hons.) and Ph.D. degrees from the University of Edinburgh. He is currently an Associate Professor and the Director of the Institute of Health and Analytics, Universiti Teknologi PETRONAS. His research interests include in neurotechnology, from device and measurement to data analysis. He received multiple awards for his research works, including the Lab on Chip Award, in 2006, the IET Nanobiotechnology Premium Award, in 2008, the IET Mountbatten Medal, in 2020, and the Top Research Scientists Malaysia Award, in 2021. He works as the Secretary of the Higher Centre of Excellence (HICoE) Council, a Governing Board Member of the INCF, and the Chair of the IEEE Circuits and Systems Society Malaysia Chapter.

DANISH M. KHAN (Member, IEEE) received the bachelor's and master's degrees in telecommunications engineering from the NED University of Engineering and Technology, Pakistan, in 2009 and 2012, respectively, and the Ph.D. degree in electrical and electronic engineering from Universiti Teknologi PETRONAS, Malaysia, in 2021. Since March 2010, he has been a Faculty Member with the Department of Telecommunications Engineering, NED University of Engineering and Technology. His research interests include signal processing, EEG, brain connectivity, seizure prediction, diagnosis of neurological disorders, and image processing.